Analytical Biochemistry 439 (2013) 65–72

Contents lists available at SciVerse ScienceDirect

Analytical Biochemistry

journal homepage: www.elsevier.com/locate/yabio

Influence of different nanozeolite particles on the sensitivity of a glucose biosensor

Ruska Nenkova [a], Jiamin Wu [b], Yahong Zhang [b], Tzonka Godjevargova [a,*]

[a] Department of Biotechnology, University "Prof. Dr. A. Zlatarov", Bourgas 8010, Bulgaria
[b] Department of Chemistry and Shanghai Key Laboratory of Molecular Catalysis and Innovative Materials, Fudan University, Shanghai 200433, People's Republic of China

ARTICLE INFO

Article history:
Received 8 January 2013
Received in revised form 3 April 2013
Accepted 4 April 2013
Available online 13 April 2013

Keywords:
Electrochemistry
Biosensor
Glucose oxidase
Nanozeolite
Glucose

ABSTRACT

Four types of nanozeolite (NZ) particles (Silicalite S-1, BEA, Silicalite S-1–DT, and BEA–DT) with different physicochemical properties have been used for preparation of the new glucose oxidase (GOD) biosensor. Cyclic voltammetric studies were carried out with four different Pt/NZ electrodes, and it was found that the electrode prepared with BEA–DT NZ showed the highest electroactivity. These cyclic voltammograms (CVs) were compared with the CVs of four Pt/NZ–GOD electrodes. The presence of the oxidoreductase (GOD) on the electrode surface was the reason for the shifting of the potential peaks and corresponding currents. The magnitudes of the cathodic peak of Pt/NZ–S-1–GOD and Pt/NZ–S-1–DT–GOD electrodes had the highest values. The surface concentration (I^*) of the adsorbed electroactive species (NZ–GOD) on the electrode was estimated according to the Brown–Anson model. The pH effect on the cathodic peak potential of Pt/NZ–GOD electrodes was investigated. The influence of different nanozeolites on sensitivity of GOD biosensors was studied. The most sensitive biosensor was obtained with NZ–S-1–DT, which had a porous surface, a higher degree of hydrophobicity, and a relatively high negative charge. The sensitivity of this electrode was 1.8044 μA L mmol^{-1}, the concentration limit was 0.8 mmol L^{-1} glucose, and the linear correlation was from 2 to 18 mmol L^{-1} glucose.

The glucose biosensor has been widely used as a clinical indicator of diabetes and in the food industry for quality control [1–5]. Indeed, glucose biosensors account for approximately 85% of the entire biosensor market. The tremendous economic prospects associated with glucose biosensors have led to a considerable amount of fascinating research and innovative detection strategies. Amperometric glucose oxidase (GOD)[1] electrodes have played a leading role in the glucose monitoring.

The most important aspects to consider in the development of electrochemical sensors are sensitivity, selectivity, long-term stability, response time, portability and low cost. So far, great efforts have been made to meet these needs through research in the development of new materials. Recently, the nanoparticle-enhancing enzyme immobilization technique has become widespread. Many kinds of nanoscale particles, such as Au [6,7], Pt [8], ZnO [9], and SiO_2 [10–12], have been used to construct nanobiosensors. A variety of glucose biosensors with high sensitivity and excellent reproducibility based on nanotechnology have been reported [13–18]. Nanomaterials provide high surface areas for enzyme loading and also afford a favorable microenvironment, helping the enzyme to retain its bioactivity. It is known that the performance of nanomaterials in any application is strongly dependent on their physicochemical characteristics. Zeolites, hydrated crystalline aluminosilicate minerals (natural or synthetic), are widely used as enzyme carriers [18]. Zeolites offer a friendly microenvironment for enzyme immobilization. Nanozeolites (NZs), which display good interaction with biomolecules, possess excellent characteristics such as a large clean surface, plentiful and tunable surface properties (e.g., adjustable surface charge and hydrophilicity/hydrophobicity), and high dispersibility in both aqueous and organic solutions [19]. These characteristics give them very high adsorption capability and a facile self-assembly character [20], making them promising candidates for the immobilization of enzymes and the construction of enzyme electrodes.

Different glucose biosensors fabricated with zeolite have been reported—zeolite dispersed in carbon paste [21], mesoporous silica MCM-41 modified glassy carbon electrode [22], and modified carbon paste electrode by incorporating ferricinium cation exchanged zeolite [23]. The development of simple and reliable procedures to immobilize and stabilize reactive enzymes on the electrode is a key issue. Ultimately, one would like to develop a reagentless glucose biosensor with a low operating potential, close to that of the redox

* Corresponding author.
E-mail address: godjevargova@yahoo.com (T. Godjevargova).

[1] *Abbreviations used:* GOD, glucose oxidase; NZ, nanozeolite; TPAOH, tetrapropylammonium; TEAOH, tetraethylammonium; S-1, silicalite-1; BEA, zeolite beta; DT, detemplation; CV, cyclic voltammogram; SEM, scanning electron microscope; FTIR, Fourier transform infrared; RSD, relative standard deviation.

0003-2697/$ - see front matter © 2013 Elsevier Inc. All rights reserved.
http://dx.doi.org/10.1016/j.ab.2013.04.004

potential of the enzyme. In this case, the electron is transferred directly from glucose to the electrode via the active site of the enzyme.

In this article, we report a simple approach to fabrication of a reagentless biosensor based on adsorption of GOD on different NZ surfaces. The method is suitable to choose the best type of zeolite for preparation of the glucose biosensor. This study aimed to investigate the influence of different NZ particles on glucose biosensor sensitivity.

Materials and methods

Apparatus and reagents

Cyclic voltammetry was performed on a PalmSens electrochemical instrument (Palm Instruments, The Netherlands). A conventional three-electrode system comprising the modified Pt disk electrode as a working electrode (surface = 0.7838 cm^2), a Pt wire as an auxiliary electrode, and an Ag/AgCl as a reference electrode was employed for all electrochemical experiments.

Tetraethylorthosilicate (TEOS, ⩾99%, Shanghai Reagent Factory), fumed silica (Aerosil 400, Shanghai Chlorine Alkali Industry), tetrapropylammonium (TPAOH, 25 wt%, Aldrich), tetraethylammonium (TEAOH, 20 wt%, Sinopharm Chemical Reagent), aluminum foil (⩾99.5%, Sinopharm Chemical Reagent), and distilled water were employed for the preparation of NZ.

NZs S-1 (silicalite-1) and BEA (zeolite beta), both before and after detemplation (DT), were used as enzyme carriers. Cross-linking of GOD from *Aspergillus niger* with specific activity of 119.3 U mg^{-1} (Fluka) and albumin from chicken egg (Sigma) was carried out with 0.7% glutaraldehyde (Fluka). All of the other reagents used for analyses were reagent grade (Fluka). Glucose stock solutions were allowed to rotate at room temperature overnight before use. Phosphate buffer solution (0.05 M, pH 5.8) was used as the supporting electrolyte in all measurements, and distilled water was used throughout.

Methods

Preparation of zeolite nanoparticles

Four NZs with different physicochemical and pore-opening properties (S-1, BEA, S-1–DT, and BEA–DT) were used as enzyme carriers. To study the micropore effects of NZs for the enzyme immobilization, S-1 and BEA were partially detemplated (S-1–DT and BEA–DT) to remove structure-directing agents of the external surface by a microwave-assisted Fenton-like oxidation method described by Hu and coworkers [24], which exposes the surface micropores of NZs. NZ S-1 was hydrothermally synthesized in the precursor solution of 1.0 SiO_2/0.39 TPAOH/21.0 H_2O in the presence of microwave irradiation, according to Ref. [25]. NZ BEA with an SiO_2/Al_2O_3 molar ratio of 60 was hydrothermally synthesized in the precursor solution of 1.0 SiO_2/0.016 Al_2O_3/0.4 TEAOH/13.09 H_2O, aged for 1 day, and the obtained mixture was then transferred into a Teflon-lined autoclave at 140 °C for 14 days to get the colloidal solution of NZ BEA. The resulting nanocrystals were cooled to room temperature and then rinsed with distilled water five times by centrifugation at 16,000 rpm.

Preparation of Pt/NZ electrode

After thorough rinsing with distilled water followed by ethanol, the electrode was cleaned electrochemically by cycling it between −0.2 and 1.45 V in aqua solution of 0.1 M H_2SO_4 at a scan rate of 0.075 V s^{-1} for 10 min or until the cyclic voltammetric characteristics for a clean Pt electrode were obtained. Four different zeolite nanoparticles (0.0025 g) were immersed in 50 μl of 0.1% albumin solution in 0.05 M phosphate buffer (pH 7.0) for 2 h. Then the mixture was centrifuged at 10,000*g* for 10 min. The supernatant was removed, and 50 μl of 0.05 M phosphate buffer without albumin (pH 7.0) was added to the zeolite nanoparticles with adsorbed albumin. A mixture of 0.7% glutaraldehyde (25 μl) and NZ with adsorbed albumin dispersed in the phosphate buffer (50 μl, pH 7.0) was applied to the electrode surface and was dried overnight at 4 °C. Cross-linking albumin kept the zeolite particles strongly adsorbed to the electrode surface. The electrochemical measurements were not influenced by the presence of albumin because it was not electroactive.

The dried Pt/NZ modified electrodes were then characterized in 0.05 M phosphate buffer (pH 5.8) using cyclic voltammetry.

Preparation of enzyme electrode

Pt electrode was cleaned electrochemically according to the procedure reported in the previous subsection. Four different zeolite nanoparticles (0.0025 g) were immersed in 0.4% GOD solution in 0.05 M phosphate buffer (pH 5.8) for 2 h. Then the mixture was centrifuged at 10,000*g* for 10 min. The supernatant was removed, and 50 μl of 0.05 M phosphate buffer without GOD (pH 7.0) was added to the zeolite nanoparticles with adsorbed enzyme. A mixture of 0.7% glutaraldehyde (25 μl) and NZ with adsorbed enzyme dispersed in the phosphate buffer (50 μl, pH 7.0) was applied to the electrode surface and was dried overnight at 4 °C. The dried Pt/NZ–GOD modified electrodes were then characterized in 0.05 M phosphate buffer (pH 5.8) at different scan rates using cyclic voltammetry.

Cyclic voltammetric and amperometric measurements with Pt/NZ and Pt/NZ–GOD electrodes

Cyclic voltammetric studies of Pt/NZ and Pt/NZ–GOD electrodes were carried out in an electrochemical cell containing 11 ml of phosphate buffer solution (0.05 M, pH 5.8) at 25 °C. The experiments were performed at potentials from 0.3 to 1 V at a scan rate of 0.1 V s^{-1}. Kinetic studies were carried out on Pt/NZ–GOD electrodes by cyclic voltammograms (CVs) as a function of scan rates varying from 0.01 to 0.2 V s^{-1}. CVs of Pt/NZ–GOD electrodes were obtained by adding glucose solution to final concentrations of 2, 7, 13, and 18 mM in the electrochemical cell, and the resulting current was recorded.

The amperometric measurements of the Pt/NZ–S-1–DT–GOD electrode were carried out by successive additions of glucose to 11 ml of 0.05 M phosphate buffer solution (pH 5.8) to a final concentration from 2 to 110 mmol L^{-1} and an applied potential of −0.1 V.

Instruments

Micropore volumes were measured by nitrogen adsorption and desorption isotherms using a Micromeritics ASAP-2010 sorptometer at liquid N_2 temperature. Scanning electron microscope (SEM) images were obtained on a Philips XL 30 microscope. Zeta potentials of NZs were detected at 25 °C by a MALVERN Zetasizer Nano ZS90. The water contact angle was measured by a DataPhysics OCA 20 instrument. A Fourier transform infrared (FTIR) spectrophotometer (Tensor 27) was used to characterize NZ particles and their interaction with the enzyme (GOD).

Results and discussion

Basic characteristics of NZ particles

The basic characteristics of the four types of NZ particles are presented in Table 1. The different types of NZ particles have different hydrophilic–hydrophobic balances and different surface charges. Both S-1–DT and BEA–DT particles have higher negative

Table 1
Basic characteristics of NZ particles.

Sample	Size[a] (nm)	Component of framework	Micropore volume (cm^3/g)	Zeta potential (mV)	Water contact angle (°)
S-1	90	All Si	0	−1.7	23.5
S-1–DT	90		0.044	−18.4	34.2
BEA	100	Si, Al	0	−26.2	14.6
BEA–DT	100	Si/Al = 28	0.094	−42.6	19.5

[a] The size of the particles was determined by SEM analysis.

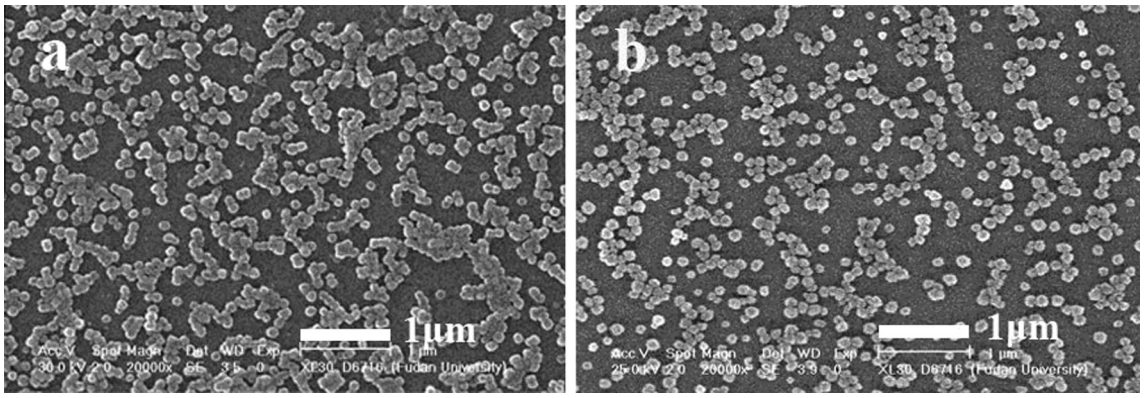

Fig.1. SEM images of two major types of NZ particles: (A) S-1–DT; (B) BEA–DT.

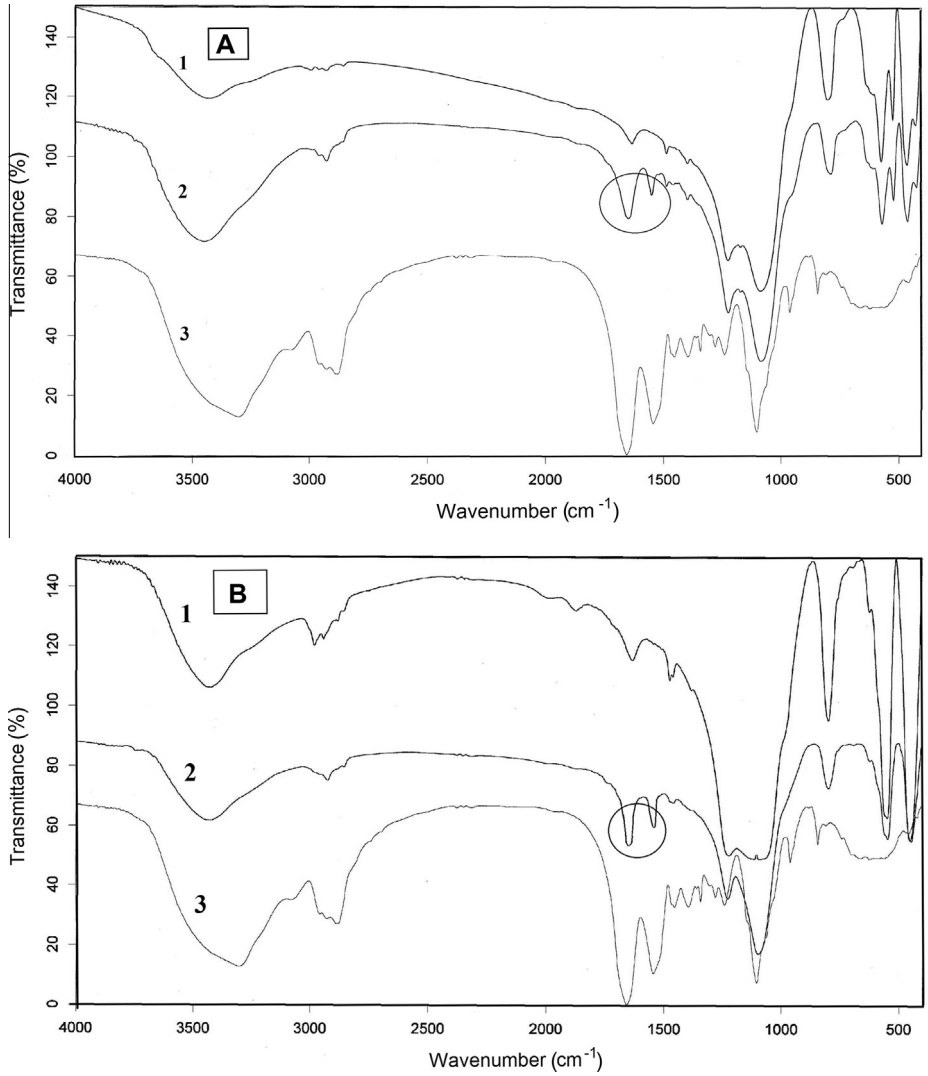

Fig.2. (A) FTIR transmission spectra of BEA–DT (1), BEA–DT–GOD (2), and GOD (3). (B) FTIR transmission spectra of S-1–DT (1), S-1–DT–GOD (2), and GOD (3).

Table 2
Basic character bands of FTIR transmission spectra of NZ particles.

Sample	Wavenumber (cm^{-1})
NZs before detemplation: S-1, BEA	Vibration from framework of NZs: 800 cm^{-1}: symmetric vibration of Si–O–Si 1000–1250 cm^{-1}: asymmetric vibration of T–O–T 550 cm^{-1}: vibration of five-membered rings in S-1 570 cm^{-1}: vibration of double six-membered rings in BEA C–H vibration (attributed to organic template TEAOH): 2987, 2942, and 2880 cm^{-1}: C–H stretching 1483, 1459, and 1396 cm^{-1}: C–H bending
NZs after detemplation: S-1–DT, BEA–DT	Vibrations from framework remain unchanged while C–H bending and stretching vibrations weaken, and the vibration of H_2O (1640 cm^{-1}) becomes stronger due to more adsorbed water in their empty channels
BEA–DT–GOD	New bands: 3288 – OH and NH stretching; 2874 – C–H symmetric stretching for CH_2; 1726 – C=O for carboxylic acid; 1652 – C=O and C–N stretching amide I; 1536 – C–N stretch and N–H bend amide II; 1220 – C–N stretching
S-1–DT–GOD	New bands: 3288 – OH and NH stretching; 2874 – C–H symmetric stretching for CH_2; 1726 – C=O for carboxylic acid; 1652 – C=O and C–N stretching amide I; 1536 – C–N stretch and N–H bend amide II; 1220 – C–N stretching

charge in comparison with S-1 and BEA and are characterized with open pores. The pore sizes of S-1–DT and BEA–DT are 5.5 and 7.5 Å, respectively. The water contact angles of S-1 and S-1–DT NZs are higher than the water contact angles of the other two types of NZ particles. Consequently, S-1 and S-1–DT NZs are more hydrophobic than BEA and BEA–DT NZs (Table 1). SEM images of two typical types of NZ particles (S-1–DT and BEA–DT) are presented in Fig. 1. They have spherical morphology and uniform sizes of 100 and 90 nm, respectively.

FTIR transmission spectra of NZs without and with immobilized GOD

The functional groups of the pure NZ particles and NZs with adsorbed GOD were demonstrated by the FTIR spectra (Fig. 2 and Table 2). The FTIR spectra of BEA and BEA–DT nanoparticles, as well as the spectra of S-1 and S-1–DT nanoparticles, were similar. Therefore, only the spectra of BEA–DT and S-1–DT nanoparticles are presented. The vibrations of the framework of BEA–DT and S-1–DT remained unchanged, whereas the C–H bending and stretching vibrations weakened, but the vibration of H_2O (1640 cm^{-1}) became stronger due to the larger amount of adsorbed water in their empty channels. The FTIR spectra of the two types of nanoparticles (BEA–DT and S-1–DT) with adsorbed GOD are presented in order to demonstrate the presence of the enzyme on the surface of the nanoparticles (Fig. 2A and B, curve 2). The appearance of new bands showed the presence of the adsorbed enzyme. The most important were the bands 1652 and 1536 cm^{-1} corresponding to the presence of –C=O and –C–N stretching amide I and –C–N stretch and N–H bend amide II groups, indicative of the peptide backbone. The spectrum of GOD (Fig. 2A and B, curve 3) is presented for comparison. The strong absorption bands of amide I and amide II, as well as NH and NH_2 bands (typical of the enzyme), indicated that GOD was successfully immobilized on the NZ surface.

CV characterization of Pt/NZ electrodes and Pt/NZ–GOD electrodes

The CVs of the four different Pt/NZ electrodes (Pt/NZ–S-1, Pt/NZ–S-1–DT, Pt/NZ–BEA, and Pt/NZ–BEA–DT) are presented in

Table 3
Cathodic peak potentials and corresponding currents of Pt/NZ and Pt/NZ–GOD electrodes.

NZ	Pt/NZ electrodes	Pt/NZ–GOD electrodes		
	E (V)	ΔI (μA)	E (V)	ΔI (μA)
BEA	0.034	56.2	0.044	95.0
BEA–DT	0.048	114.7	0.054	104.8
S-1	0.044	15.30	0.049	130.39
S-1–DT	0.064	71.72	0.049	135.55

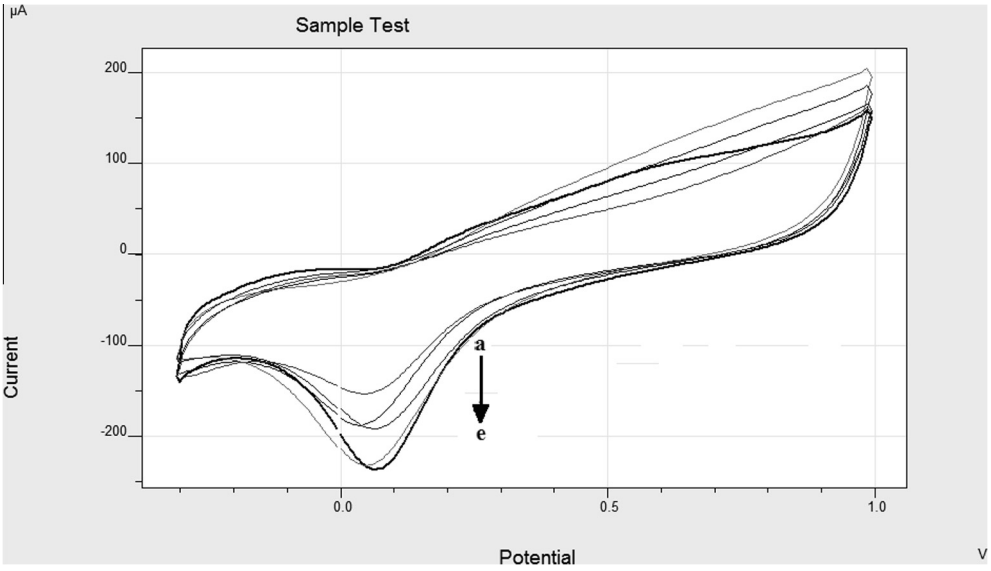

Fig.3. CVs of Pt/NZ–S-1 (a), Pt/NZ–S-1–DT (b), Pt/NZ–BEA (c), and Pt/NZ–BEA–DT (d) electrodes and Pt electrode (e) in a 0.05 M phosphate buffer (pH 5.8) at a potential from −0.3 to 1 V and a scan rate of 0.1 V s^{-1}.

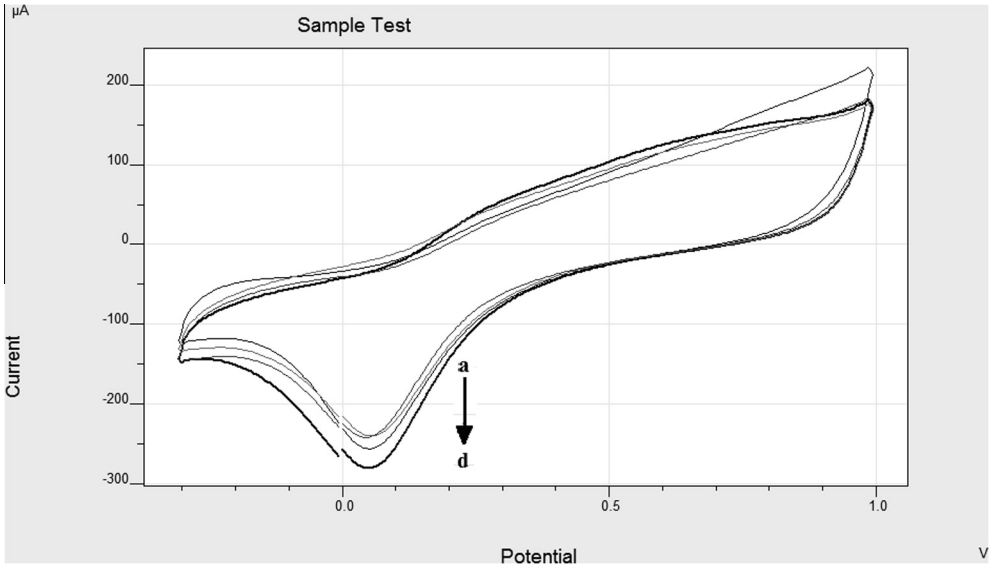

Fig.4. CVs of Pt/NZ–BEA–GOD (a), Pt/NZ–BEA–DT–GOD (b), Pt/NZ–S-1–GOD (c), and Pt/NZ–S-1–DT–GOD (d) electrodes in a 0.05 M phosphate buffer (pH 5.8) at a potential from −0.3 to 1 V and a scan rate of 0.1 V s^{-1}.

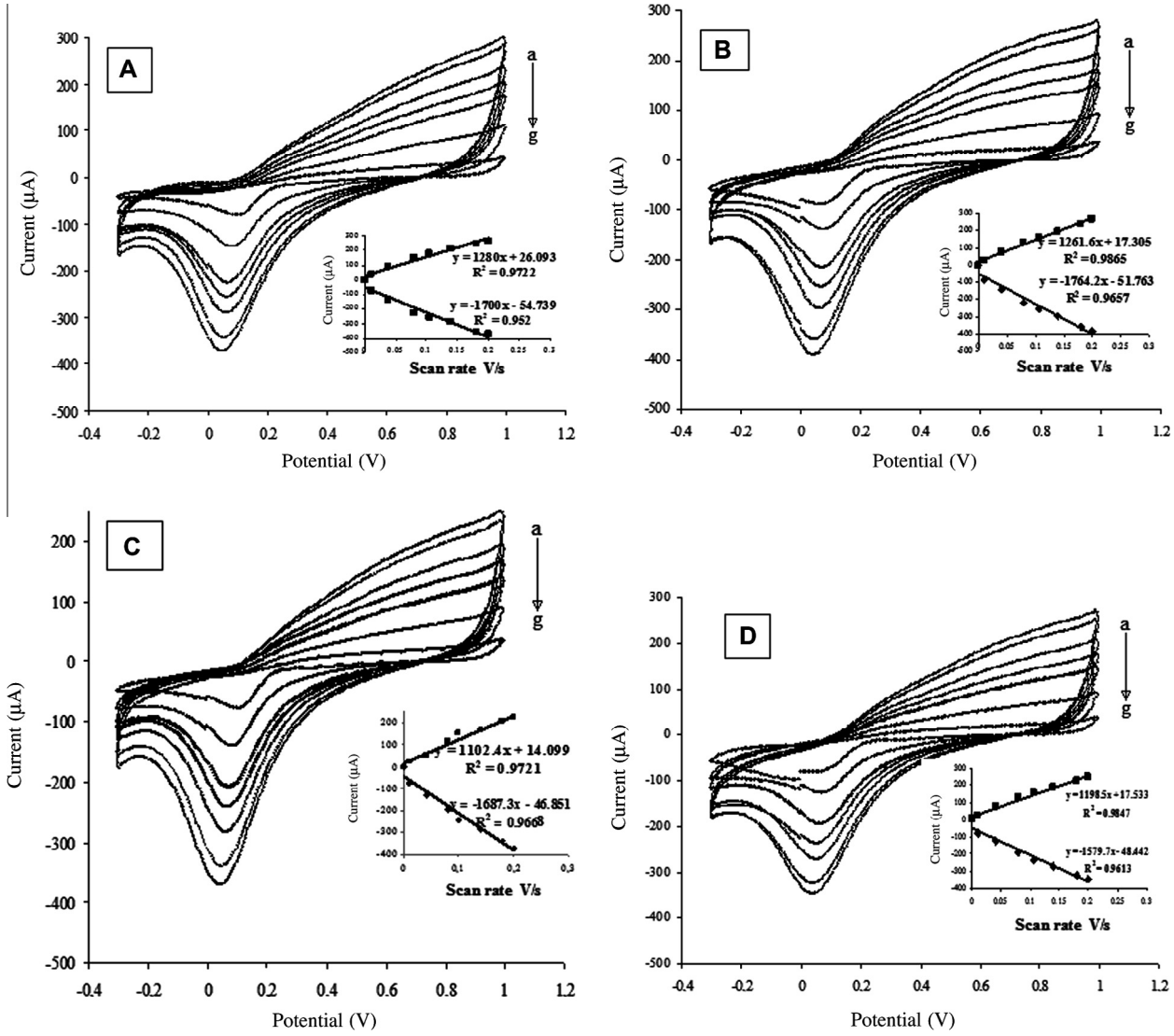

Fig.5. CVs of Pt/NZ–S-1–GOD (A), Pt/NZ–S-1–DT–GOD (B), Pt/NZ–BEA–GOD (C), and Pt/NZ–BEA–DT–GOD (D) electrodes in a 0.05 M phosphate buffer (pH 5.8) at scan rates from 0.01 to 0.2 V s^{-1} (a–g). Insets show the plots of peak currents of the same electrodes versus scan rates.

Fig. 3. It is noteworthy that in comparison with the bare Pt electrode (Fig. 3, curve e), using different NZ particles in preparation of the electrodes resulted in different CVs. They exhibited one cathodic peak at 0.05 V and a strong shift of the anodic curve at 0.8 V. The CVs showed that the peak potentials and corresponding peak currents varied depending on the type of zeolite nanoparticles. The magnitude of the cathodic peak of the Pt/NZ–BEA–DT electrode had the highest value (ΔI = 114.7 μA), whereas the lowest value corresponded to the Pt/NZ–S-1 electrode (ΔI = 15.3 μA) (Table 3). Obviously, the electrode with BEA–DT NZs was more electroactive. The open micropores of the BEA–DT NZs in the detemplating process can transfer cations by an ion exchange process between the micropores and the solution, thereby favoring the electroactivity of the electrode. The CVs of these four Pt/NZ electrodes were compared with the CVs of four Pt/NZ–GOD electrodes (Pt/NZ–S-1–GOD, Pt/NZ–S-1–DT–GOD, Pt/NZ–BEA–GOD, and Pt/NZ–BEA–DT–GOD) (Fig. 4). The presence of the oxidoreductase (GOD) on the electrode surface was the reason for the shifting of the peak potentials (E, V) and the change of peak magnitudes (ΔI, μA) (Table 3). In this case, the magnitude of the cathodic peaks of Pt/NZ–S-1–GOD (Fig. 4, curve c) and Pt/NZ–S-1–DT–GOD (Fig. 4, curve d) electrodes had the highest values, ΔI = 130.39 and 135.55 μA, respectively (Table 3). The better electroactivity of these electrodes is probably due to the greater amount of the immobilized enzyme and the good enzyme conformation on the NZ particles S-1 and S-1–DT. The two types of NZs have the lowest negative electric charge. These results are completely consistent because it is known that the pI of GOD is 4.2. At a pH below the value of the pI, the proteins carry a net positive charge; above their pI, they carry a net negative charge. In our case, the GOD adsorption on the NZs was carried out at pH 5.8. Therefore, the charge of the enzyme molecules was negative. This means that fewer enzyme molecules are adsorbed on the negatively charged NZ particles BEA and BEA–DT and vice versa. Hence, the amount of the immobilized enzyme reflected on the values of the cathodic peak magnitude of the enzyme electrodes.

Furthermore, the results were also in accordance with the hydrophilicity of the NZ particles. It is known that the hydrophobic surfaces adsorb more proteins than the hydrophilic surfaces. S-1 and S-1–DT NZs were estimated to be the most hydrophobic NZ particles because their water contact angles had the highest values (Table 1). Consequently, the electrodes prepared with these two types of NZs adsorbed more enzyme molecules and showed higher electroactivity.

Kinetic studies of Pt/NZ–GOD electrodes

Determination of surface concentration of absorbed electroactive species

The effect of the scan rates on the currents of the four Pt/NZ–GOD electrodes (Pt/NZ–S-1–GOD, Pt/NZ–S-1–DT–GOD, Pt/NZ–BEA–GOD, and Pt/NZ–BEA–DT–GOD) was studied. The scan rates varied from 0.01 to 0.2 V s^{-1} (Fig. 5A–D). The cathodic and anodic peak currents increased linearly with the increase of the scan rates in that range (Fig. 5A–D, insets). The response was stable, with no changes observed, after 20 potential cycles. The equations of these linear dependences are presented in Table 4. As can be seen, the electrodes prepared with S-1–DT and S-1 NZs have the greatest slope of the cathodic linear dependence and are the most sensitive.

The number of electrons transferred was estimated from the CVs of Pt/NZ–GOD electrodes and was calculated using the equation

$$/Ep - Ep_{1/2}/ = 2.20\ RT/nF = 56.5/n, \quad (1)$$

where Ep is the maximum cathodic peak potential, $Ep_{1/2}$ is half of the maximum cathodic peak potential, R is the gas constant (8.314 J (mol K)$^{-1}$), T is the absolute temperature (298 K) of the system, F is the Faraday constant (96.584 C mol^{-1}), and n represents

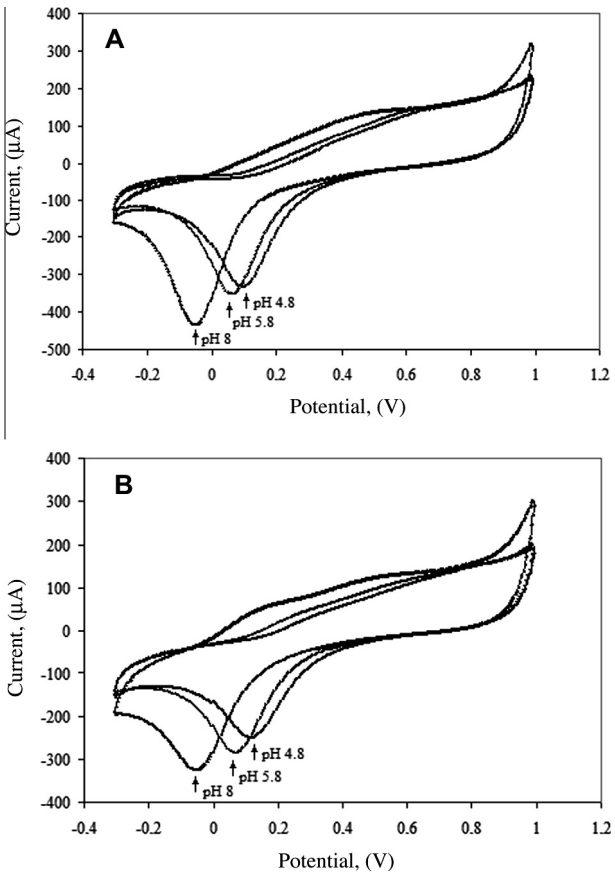

Fig.6. Influence of pH on CVs of Pt/NZ–S-1–GOD (A) and Pt/NZ–BEA–DT–GOD (B) electrodes at a scan rate of 0.1 V s^{-1}.

Table 4
Mathematical dependences of kinetic studies of Pt/NZ–GOD electrodes.

Type of electrodes	Linear equation between cathodic peak current (y) and potential scan rate (x)	I^* (mol cm^{-2})	Linear equation between cathodic peak current (y) and glucose concentrations (x)
Pt/NZ–S-1–GOD	$y = -1700x - 56.911$ $R^2 = 0.947$	0.566	$y = -1.2075x - 1.4253$ $R^2 = 0.9963$
Pt/NZ–S-1–DT–GOD	$y = -1764x - 51.763$ $R^2 = 0.9657$	0.597	$y = -1.8044x - 5.7$ $R^2 = 0.9923$
Pt/NZ–BEA–GOD	$y = -1687.3x - 46.851$ $R^2 = 0.9668$	0.522	$y = -0.787x - 0.5449$ $R^2 = 0.9890$
Pt/NZ–BEA–DT–GOD	$y = -1579.7x - 48.442$ $R^2 = 0.9613$	0.535	$y = -1.4623x - 0.6233$ $R^2 = 0.9991$

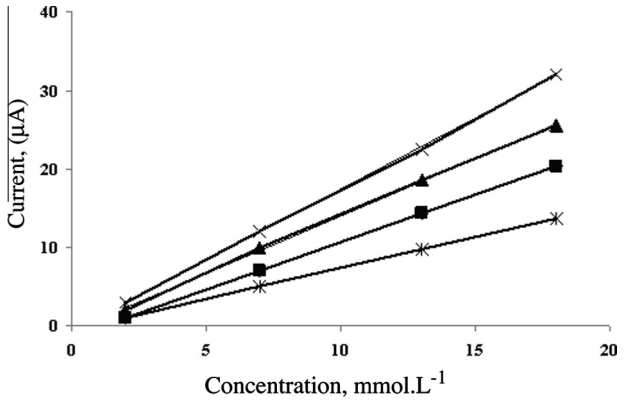

Fig.7. Linear correlation between current and glucose concentration, obtained on basis of CVs of biosensors with different types of NZs: Pt/NZ–S-1–DT-GOD (x), Pt/NZ–BEA–DT–GOD (▲), Pt/NZ–S-1–GOD (■), and Pt/NZ–BEA–GOD (∗) electrodes in 0.05 M phosphate buffer (pH 5.8) at a scan rate of 0.1 V s^{-1}.

the number of electrons transferred. It was found to be a two-electron transfer system for Pt/NZ–GOD electrodes.

The surface concentration (I^*) of the absorbed electroactive species (NZ–GOD), therefore, could be estimated from the plot of I_p versus v, in accordance with the Brown–Anson model [26], using the equation

$$I_p = n^2F^2I^*Av/4RT, \quad (2)$$

where I_p represents the cathodic peak current at a different scan rate, A is the surface area of the electrode (0.7838 cm^2), v is the scan rate (V s^{-1}), I^* is the surface concentration of the absorbed electroactive species, and F, R, and T are the same as in Eq. (1). The surface concentration of electroactive species was calculated on the base of the CVs of the Pt/NZ–GOD electrodes and Eq. (2) and are presented in Table 4. The highest concentration (I^*) of the enzyme on the electrode surface corresponded to the electrodes prepared by NZ–S-1 and NZ–S-1–DT (i.e., the nanoparticles with higher hydrophobicity and lower negative charge). The values of I^* correlate completely with the above-discussed results concerning the relation between the main characteristics of the NZ particles and the electroactivity of the Pt/NZ and Pt/NZ–GOD electrodes.

pH effect on CVs of Pt/NZ–GOD electrodes

The pH effect of the solution on the voltammetric response of the four Pt/NZ–GOD electrodes was studied (Fig. 6). The results showed that with the increase of pH, the cathodic peak of the Pt/NZ–GOD electrodes shifted to negative potential values. The CVs of only the Pt/NZ–S-1–GOD and Pt/NZ–BEA–DT–GOD electrodes are presented in Fig. 6 because they have the lowest and highest negative charges, respectively. The pH effect on the value of the cathodic peak magnitude was also observed (Fig. 6). The electrodes Pt/NZ–S-1–GOD and Pt/NZ–S-1–DT–GOD with a higher amount of immobilized enzyme showed greater pH influence.

Amperometric response of biosensor

The linear dependence on glucose concentration (2–18 mmol L^{-1}) of the CV curves of all four Pt/NZ–GOD electrodes is presented in Fig. 7. The derived equations of the linear correlation are presented in Table 4. Obviously, the Pt/NZ–BEA–GOD electrode had the lowest response current and sensitivity, 0.787 μA L $mmol^{-1}$. That was indicative that the modified surface contained a small amount of immobilized enzyme (I^* = 0.522 mol cm^{-2}); thus, the amount of H_2O_2 gained in the reaction with glucose was also small. The obtained results indicated that the Pt/NZ–S-1–DT–GOD electrode, prepared with NZ particles with porous surface with the highest degree of hydrophobicity and relatively small negative charge, was the most sensitive. The sensitivity of this electrode was 1.8044 μA L $mmol^{-1}$. This type of NZ might create a suitable microenvironment that benefits the exposition of the enzyme active center and increases the response current. This study proves that the enzyme immobilized on different zeolite surfaces has distinct effectiveness.

An amperometric study of the most sensitive glucose Pt/NZ–S-1–DT–GOD electrode was carried out. Fig. 8, inset a, shows the current–time responses on Pt/NZ–S-1–DT–GOD electrode on successive additions of glucose to 0.05 M phosphate buffer solution (pH 5.8) at an applied potential of −0.1 V. With the increase of the glucose concentration, the amperometric responses increased linearly in two ranges: first range from 2 to 18 mmol L^{-1} with

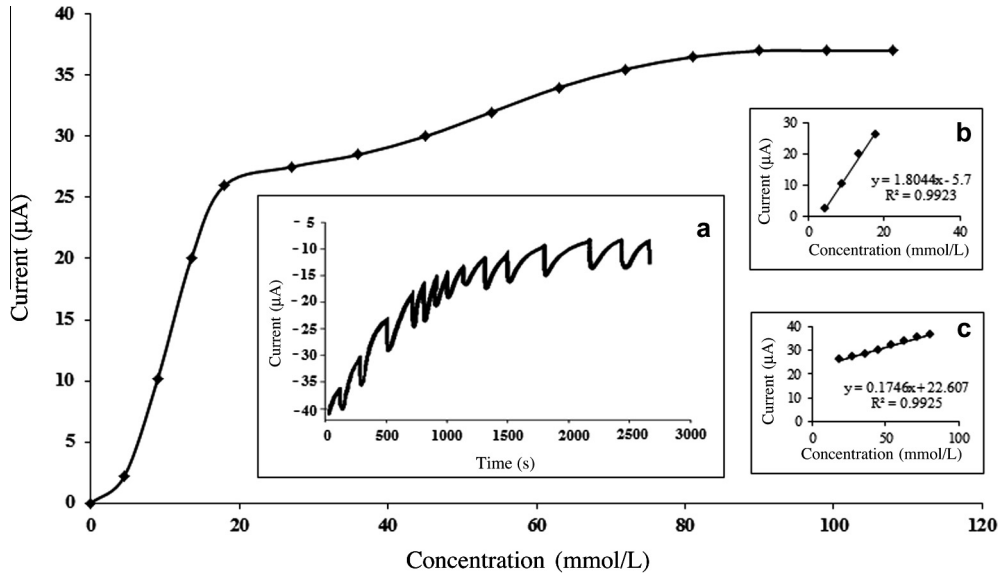

Fig.8. Calibration curve for glucose using Pt/NZ–S-1–DT–GOD electrode. Insets: (a) current–time response of the Pt/NZ–S-1–DT–GOD electrode to glucose in 0.05 M phosphate buffer solution (pH 5.8) at applied potential of −0.1 V; (b) linear correlation between current and concentration of glucose from 2 to 18 mmol L^{-1}; (c) linear correlation between current and concentration of glucose from 18 to 90 mmol L^{-1}.

Table 5
Performance of Pt/NZ–S-1–DT–GOD biosensor compared with biosensors previously reported in literature.

Material	Linearity	Sensitivity	Reference
Fe_3O_4/SPCE	0–33.3 mM	1.74 μA mM^{-1}	Lu and Chen [27]
Au–CH/Pt	0.5–16 mM	0.555 μA mM^{-1}	Wu et al. [28]
CNT–CH	0–7.8 mM	0.52 μA mM^{-1}	Liu et al. [17]
CH–ZrO_2	1.25×10^{-2} to 9.5 mM	0.028 μA mM^{-1}	Yang et al. [29]
Nafion–SWCNHs	0–6.0 mM	1.06 μA mM^{-1}	Liu et al. [30]
Pt/NZ–S-1–DT–GOD	2–18 mmol L^{-1}	1.8044 μA L $mmol^{-1}$	Current work

Note: SPCE, screen-printed carbon electrode; CH, chitosan; CNT, carbon nanotube; SWCNHs, single-walled carbon nanohorns.

linear equation $I = 1.8044 \cdot C_{glucose} - 5.7$ (μA, mmol L^{-1}, $R^2 = 0.9923$) (Fig. 8, inset b); second range from 18 to 90 mmol L^{-1} with linear equation $I = 0.1746 \cdot C_{glucose} + 22.61$ (μA, mmol L^{-1}, $R^2 = 0.9925$) (Fig. 8, inset c). The detection limit was 0.8 mmol L^{-1} at a signal-to-noise ratio of 3. The remarkable sensitivity would couple with very high selectivity (e.g., negligible interferences from ascorbic and uric acids, acetaminophen, and cysteine at +0.10 V vs. Ag/AgCl). It is known that the detection of H_2O_2 by its oxidation at a platinum electrode requires a potential of +0.5 to +0.6 V (vs. Ag/AgCl) and, hence, is subject to interference by ascorbic and uric acids [18].

The obtained results were compared with the results reported in other similar articles (Table 5). Obviously, our results are comparable to the results published by other authors. The reproducibility and storage stability of the Pt/NZ–S-1–DT–GOD electrode were examined to prove the precision and practicability of this method. The relative standard deviation (RSD) of the biosensor response to 9 mmol L^{-1} glucose was 4.0% ($n = 6$). The RSD for the detection of 9 mmol L^{-1} glucose on the five newly fabricated biosensors was 5.3%. Those results showed that the biosensor exhibited good reproducibility. When the enzyme electrode was not used, it was wrapped with a piece of thin plastic film and stored at 4 °C. After 40 days, the biosensor kept 80% of its initial current response to glucose.

Conclusion

The obtained results showed that the performance of the Pt/NZ–GOD electrode was influenced by the type of NZs included in the enzyme composition. The most sensitive electrode was obtained with NZ–S-1–DT particles with a porous surface, a higher degree of hydrophobicity, and a relatively small negative charge. The greater enzyme loading may be the main reason for the high enzyme activity of GOD. It still requires more efforts to further explore the mechanism underlying the interaction between NZs and enzymes so as to make clear which factor plays a more important role for enzyme loading, conformation, and activity.

Acknowledgments

The authors gratefully acknowledge the Bulgarian Ministry of Education and the National Science Fund (project DNTS–01/09) for their financial support and encouragement of the scientific research work in state universities.

References

[1] E. Bakker, Electrochemical sensors, Anal. Chem. 76 (2004) 3285–3298.
[2] M.I. Prodromidis, M.I. Karayannis, Enzyme based amperometric biosensors for food analysis, Electroanalysis 14 (2002) 241–261.
[3] Y.H. Yang, H.F. Yang, M.H. Yang, Y.L. Liu, G.L. Shen, R.Q. Yu, Amperometric glucose biosensor based on a surface treated nanoporous ZrO_2/chitosan composite film as immobilization matrix, Anal. Chim. Acta 525 (2004) 213–220.
[4] A. Kros, M. Gerritsen, V. Sprakel, N. Sommerdijk, J. Jansen, R. Nolte, Silica-based hybrid materials as biocompatible coatings for glucose sensors, Sens. Actuators, B 81 (2001) 68–75.
[5] Y. Xian, Y. Hu, F. Liu, Y. Xian, H. Wang, L. Jin, Glucose biosensor based on Au nanoparticles–conductive polyaniline nanocomposite, Biosens. Bioelectron. 21 (2006) 1996–2000.
[6] Y. Xiao, F. Patolsky, E. Katz, J. Hainfeld, I. Willner, "Plugging into enzymes": nanowiring of redox enzymes by a gold nanoparticle, Science 299 (2003) 1877–1881.
[7] Y. Du, X.L. Luo, J.J. Xu, H.Y. Chen, A simple method to fabricate a chitosan–gold nanoparticles film and its application in glucose biosensor, Bioelectrochemistry 70 (2007) 342–347.
[8] T. Selvaraju, R. Ramaraj, Electrochemically deposited nanostructured platinum on nafion coated electrode for sensor applications, J. Electroanal. Chem. 585 (2005) 290–300.
[9] T. Kong, Y. Chen, Y. Ye, K. Zhang, Z. Wang, X. Wang, An amperometric glucose biosensor based on the immobilization of glucose oxidase on the ZnO nanotubes, Sens. Actuators, B 138 (2009) 344–350.
[10] W. Jia, K. Wang, Z. Zhu, H. Song, X. Xia, One-step immobilization of glucose oxidase in a silica matrix on a Pt electrode by an electrochemically induced sol–gel process, Langmuir 23 (2007) 11896–11900.
[11] H. Yang, Y. Zhu, Size dependence of SiO_2 particles enhanced glucose biosensor, Talanta 68 (2006) 569–574.
[12] X. Luo, J. Xu, W. Zhao, H. Chen, Glucose biosensor based on ENFET doped with SiO_2 nanoparticles, Sens. Actuators, B 97 (2004) 249–255.
[13] J. Wang, M. Musameh, Carbon nanotube/Teflon composite electrochemical sensors and biosensors, Anal. Chem. 75 (2003) 2075–2079.
[14] Y. Lin, F. Lu, Y. Tu, Z. Ren, Glucose biosensors based on carbon nanotube nanoelectrode ensembles, Nano Lett. 4 (2004) 191–195.
[15] S. Hrapovic, Y. Liu, K.B. Male, J.H.T. Luong, Electrochemical biosensing platforms using platinum nanoparticles and carbon nanotubes, Anal. Chem. 76 (2004) 1083–1088.
[16] G. Liu, Y. Lin, Amperometric glucose biosensor based on self-assembling glucose oxidase on carbon nanotubes, Electrochem. Commun. 8 (2006) 251–256.
[17] Y. Liu, M. Wang, F. Zhao, Z. Xu, S. Dong, The direct electron transfer of glucose oxidase and glucose biosensor based on carbon nanotubes/chitosan matrix, Biosens. Bioelectron. 21 (2005) 984–988.
[18] J. Dong, X. Zhou, H. Zhao, J. Xu, Y. Sun, Reagentless amperometric glucose biosensor based on the immobilization of glucose oxidase on a ferrocene@NaY zeolite composite, Microchim. Acta 174 (2011) 281–288.
[19] W. Shan, Y.H. Zhang, W.L. Yang, C. Ke, Z. Gao, Y.E. Ye, Y. Tang, Electrophoretic deposition of nanosized zeolites in non-aqueous medium and its application in fabricating thin zeolite membranes, Microporous Mesoporous Mater. 69 (2004) 35–42.
[20] Y.H. Zhang, F. Chen, W. Shan, J.H. Zhuang, A.G. Dong, W.B. Cai, Y. Tang, Fabrication of ultrathin nanozeolite film modified electrodes and their electrochemical behavior, Microporous Mesoporous Mater. 65 (2003) 277–285.
[21] J. Wang, A. Walcarius, Zeolite containing oxidase-based carbon paste biosensors, J. Electroanal. Chem. 404 (1996) 237–242.
[22] Z.H. Dai, J. Ni, X.H. Huang, G.F. Lu, J.C. Bao, Direct electrochemistry of glucose oxidase immobilized on a hexagonal mesoporous silica–MCM-41 matrix, Bioelectrochemistry 70 (2007) 250–256.
[23] S. Serban, N.E. Murr, Use of ferricinium exchanged zeolite for mediator stabilization and analytical performances enhancement of oxidase-based carbon paste biosensors, Anal. Lett. 36 (2003) 1739–1753.
[24] Y.Y. Hu, Y.H. Zhang, Y. Tang, Rapid detemplation of nanozeolite *β*: microwave-assisted Fenton-like oxidation, RSC Adv. 2 (2012) 6036–6041.
[25] Y.Y. Hu, C. Liu, Y.H. Zhang, N. Ren, Y. Tang, Microwave-assisted hydrothermal synthesis of nanozeolites with controllable size, Microporous Mesoporous Mater. 119 (2009) 306–314.
[26] A.J. Bard, L.R. Faulkner, Electrochemical Methods: Fundamentals and Applications, second ed., John Wiley, New York, 2000.
[27] B.W. Lu, W.C. Chen, A disposable glucose biosensor based on drop-coating of screen-printed carbon electrodes with magnetic nanoparticles, J. Magn. Magn. Mater. 304 (2006) e400–e402.
[28] B.Y. Wu, S.H. Hou, F. Yin, J. Li, Z.X. Zhao, J.D. Huang, Q. Chen, Amperometric glucose biosensor based on layer-by-layer assembly of multilayer films composed of chitosan, gold nanoparticles and glucose oxidase modified Pt electrode, Biosens. Bioelectron. 22 (2007) 838–844.
[29] Y. Yang, H. Yang, M. Yang, Y. Liu, G. Shen, R. Yu, Amperometric glucose biosensor based on a surface treated nanoporous ZrO_2/chitosan composite film as immobilization matrix, Anal. Chim. Acta 525 (2004) 213–220.
[30] X. Liu, L. Shi, W. Niu, H. Li, G. Xu, Amperometric glucose biosensor based on single-walled carbon nanohorns, Biosens. Bioelectron. 23 (2008) 1887–1890.